Construction and Building Materials 111 (2016) 805–813

Contents lists available at ScienceDirect

Construction and Building Materials

journal homepage: www.elsevier.com/locate/conbuildmat

Influence of chloride concentration and pre-passivation on the pitting corrosion resistance of low-alloy reinforcing steel in simulated concrete pore solution

Jinjie Shi *, Wei Sun, Jinyang Jiang, Yamei Zhang

Jiangsu Key Laboratory of Construction Materials, School of Materials Science and Engineering, Southeast University, Nanjing 211189, China

HIGHLIGHTS

- New low-alloy steel has been developed for application in concrete.
- The passive film could improve the pitting corrosion resistance.
- The compact Cr-enriched rust layer delays the propagation of corrosion pits for low-alloy steel.

ARTICLE INFO

Article history:
Received 11 October 2015
Received in revised form 5 January 2016
Accepted 21 February 2016
Available online 21 March 2016

Keywords:
Concrete
Low-alloy steel
Pitting corrosion
Cyclic potentiodynamic polarization
Passive film

ABSTRACT

The effect of chloride concentration and pre-passivation on the pitting corrosion resistance of low-alloy steel and conventional low-carbon steel in simulated concrete pore solution was investigated using electrochemical techniques and surface analysis measurements. The results show that the passive film could enhance the pitting corrosion resistance for both investigated steels. Low-alloy steel exhibits slightly lower pitting corrosion resistance at low chloride concentration compared to low-carbon steel, regardless of the passivation condition. However, at high chloride concentration, low-alloy steel shows higher pitting corrosion resistance due to the formation of Cr-enriched protective rust layer.

1. Introduction

In severe environments, the main process that may cause premature degradation of the service life of reinforced concrete structures is steel corrosion. When steel is exposed to alkaline pore solution of concrete, protective passive film is formed on steel surface. However, carbonation and chloride attack can breakdown this passive film and finally lead to active corrosion of steel [1,2]. So far, many techniques have been employed to mitigate steel corrosion [3–8] in reinforced concrete. Due to the high performance/cost ratio, low-alloy reinforcing steels with a small amount of corrosion-resistant alloying elements have attracted more and more attention [6–15].

It was found that low-alloy steel with 0.13 wt.% Cu and 0.10 wt.% Cr exhibited 2–3 times lower corrosion rate than plain carbon steel when exposed to simulated concrete pore solutions with 3.5 wt.% NaCl, due to the formation of very stable, adherent and protective rust layer on the surface of low-alloy steel [7]. It was confirmed that the alloying elements (Ti and V) induced grain refinement was the main reason for the improved corrosion resistance of low-alloyed mild steels in saturated calcium hydroxide [9]. Moreover, it was reported that iron/steel with different contents of phosphorus exhibited good corrosion resistance, which was related to the formation of inhibitive phosphate [13,14].

It must be emphasized, however, in some cases unexpected lower corrosion resistance for low-alloy steel was identified compared with low-carbon steel in the literature [8,16]. It was reported that during the initial period of exposure to simulated concrete pore solutions with 3.5 wt.% NaCl, low-alloy steel (0.26 wt.% Cu + 0.07 wt.% Cr + 0.10 wt.% Ni) exhibited inferior resistance to corrosion compared with thermo-mechanically treated steel. However, after long-term exposure, this trend was reversed [8]. This was primarily explained by its especial microstructure of low-alloy steel, which was more susceptible to chloride-induced corrosion [6,16,17]. Therefore, on the basis of the results obtained, it is

* Corresponding author.
E-mail address: jinjies@126.com (J. Shi).

http://dx.doi.org/10.1016/j.conbuildmat.2016.02.107
0950-0618/

reasonable to deduce that the corrosion resistance of low-alloy steel is not only dependent upon the alloying elements, but also on the altered microstructure of steel [6–9,11,12,16,17].

Cyclic potentiodynamic polarization (CPP) technique has been widely used to achieve the pitting corrosion resistance of reinforcing steels by many researchers [18–26]. It is well known that passive layer will be naturally formed on steel surface when exposed to alkaline solution. In the pore solution of concrete, it appears that in most cases sufficient time was provided for the formation of passive film before the steel was attacked by chlorides and carbonation [27]. However, there are no universal standards for considering if steel should be naturally passivated in alkaline solution prior to CPP measurements. Therefore, most of the researchers conducted CPP measurements for reinforcing steel before the formation of stable passive film [10,20,23,25], while only a few studies employed CPP measurements after steel was fully passivated [21,26]. Additionally, few previous works so far have focused on the influence of naturally formed passive film on chloride-induced pitting corrosion resistance of steel [18,19], although it is generally recognized that well-formed passive film plays a vital role on the pitting corrosion resistance of steel in concrete [27–31].

In this study, the chloride-induced pitting corrosion resistance and corrosion morphology of low-alloy steel in simulated concrete pore solution with various chloride concentrations were investigated. Furthermore, the effects of naturally formed passive film on the pitting corrosion resistance were also evaluated.

2. Experimental

2.1. Materials

The low-alloy hot-rolled deformed steel (labeled as LA steel) was specially designed through the optimization of alloy composition and technological process. The conventional low-carbon hot-rolled deformed steel (labeled as LC steel) was also tested for comparison purpose. Compared with LC steel, LA steel contains 0.859 wt.% alloying element Cr and a very small amount of alloying elements Cu and Ni (Table 1). In order to meet the requirements of carbon equivalent, the content of Mn in LA steel is obviously lower than that in LC steel.

The cylinder steel specimens with the thickness of 10 mm were cut from deformed rebar. The cross-section of steel specimens were wet ground with SiC grinding paper successively to 1200 grits, and then polished with diamond polishing agent. After that, the polished steel specimens were cleaned with ethanol, and then dried for metallographic analysis and electrochemical measurements.

Fig. 1 shows the optical micrographs of the microstructure, observed under an Olympus optical microscope, of LC and LA steels after etching in 4% nital solution (4 ml HNO_3 mixed with 96 ml ethanol). Both LC and LA steels show similar metallographic structure with two dominant phases, ferrite (lighter area) and pearlite (darker area), which are the typical phases in reinforcing steel widely used in civil engineering [32]. In addition, it can be seen that the grain size of LA steel (Fig. 1b) is larger than that of LC steel (Fig. 1a) due to the different heat treatment processes. The addition of ferritizer element Cr results in higher transformation temperature for LA steel, which thus promotes the growth of ferrite grain at high-temperature zone [33].

The simulated concrete pore solution (SCPS) used in this study was 0.1 mol/L NaOH + 0.2 mol/L KOH + 0.1 mol/L $Ca(OH)_2$ + 0.003 mol/L $CaSO_4$ [28]. The pH of SCPS was 13.3 under normal room temperature. Excessive amounts of undissolved $Ca(OH)_2$ in SCPS was used to compensate the pH reduction by carbonation during the period of electrochemical testing [18,21,28]. All reagents used were of analytical grade, and the deionized water was used as the solvent.

2.2. Electrochemical measurements

The classical three-electrode set-up was used for electrochemical measurements. Saturated calomel electrode (SCE) and platinum electrode were used as the reference electrode and the counter electrode, respectively. The exposed area of steels was fixed to 1 cm^2 in the corrosion cell. PARSTAT 2273 potentiostat was employed to perform the electrochemical measurements. All potentials mentioned herein are referred to the saturated calomel electrode (SCE). Electrochemical impedance spectroscopy (EIS) measurements were conducted at the open circuit potentials with the AC perturbation amplitude of 10 mV in the frequency range from 100 kHz to 10 mHz. Cyclic potentiodynamic polarization (CPP) curves were measured from 200 mV_{SCE} negative to E_{corr}, then up to +800 mV_{SCE}, and finally reversed to E_{corr} [21]. The scan rate of CPP measurements was 2 mV/s [21–23].

In this study, steels without passivation and with pre-passivation for 10 days in chloride-free SCPS were prepared before CPP measurements. For the case without passivation, steels were all immersed in chloride-free SCPS for 1 h to reach stabilization of the open circuit potentials. It should be noted that stable passive film cannot be formed during such short exposure time [19,27,28]. Afterwards, steels were exposed to SCPS with three different NaCl concentrations of 0.1 M (lower than the threshold chloride content), 0.3 M (close to the threshold chloride content) and 1.0 M (high chloride content in severe marine environment) for characterization of pitting corrosion resistance [20]. For pre-passivation case, steels were immersed in chloride-free SCPS for 10 days to form a stable passive film prior to the addition of chlorides [19,21,27,28]. Afterwards, the experimental procedure for the characterization of pitting corrosion resistance was the same as the non-passivation case. Triple steel specimens were prepared for each case in order to ensure the reproducibility of results.

2.3. Surface morphology of corrosion products

After the electrochemical measurements, steel specimens were rinsed with deionized water in order to remove the loose precipitates and retain the corrosion products on steel surface. Then, specimens were dried and stored in a desiccator for microstructure observation.

Table 1
Chemical composition of LC and LA steels.

Steel type	Chemical composition (wt.%)									
	Fe	C	Si	Mn	P	S	V	Cr	Cu	Ni
LC	Bal.	0.22	0.53	1.44	0.025	0.022	0.038	–	–	–
LA	Bal.	0.199	0.654	0.571	0.0267	0.0076	0.0323	0.859	0.056	0.033

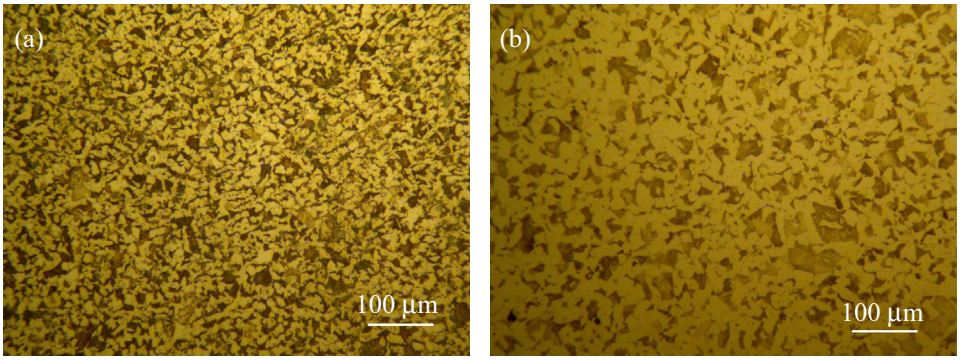

Fig. 1. Optical micrographs of etched (a) LC steel and (b) LA steel.

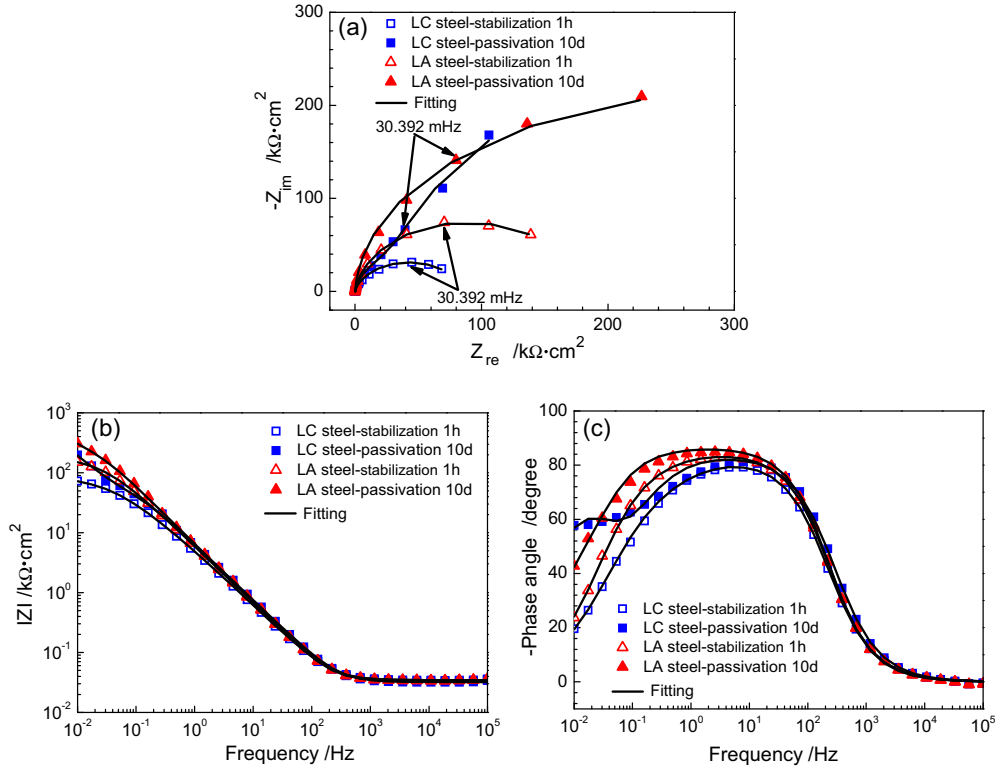

Fig. 2. EIS diagrams of LC and LA steels before and after 10 days of passivation in SCPS. (a) Nyquist plots, and (b and c) Bode plots.

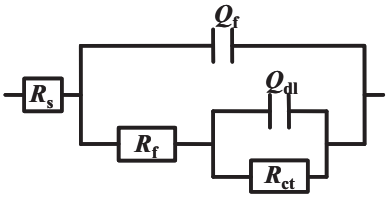

Fig. 3. Equivalent circuit proposed to fit the impedance spectra.

The surface morphology of corrosion products was observed under optical microscopy (OM) and Sirion field emission scanning electron microscopy (FESEM). Energy dispersive X-ray spectrometry (EDS) was also performed so as to identify the chemical composition of different corrosion products. The distribution of characteristic elements on the cross-section of steel specimen was detected by electron probe micro analyzer (EPMA) at an acceleration voltage of 15 kV. The 3D profiles of corrosion products and corrosion pits were observed using confocal laser scanning microscopy (CLSM) with the resolution of 0.18 μm.

3. Results and discussion

3.1. Passivation behavior

It is evident from Fig. 2a that, after 10 days of passivation in SCPS, the diameter of the low-frequency capacitive loop for both LC and LA steels is increased. Moreover, the low-frequency impedance modulus of both steels is increased (Fig. 2b), and the phase angle shifts upward with the peaks broadened (Fig. 2c). Accordingly, it indicates that passive film has been formed on the surface of both steels, and the corrosion resistance is increased significantly [30,31].

In order to extract quantitative electrochemical information from EIS images, many equivalent circuits have been used to analyze EIS data of passive film formed on steel surface [30,31,34–37]. In this study, a suitable equivalent circuit shown in Fig. 3 was selected. In this equivalent circuit, R_s is the resistance of simulated solution. R_{ct} is the charge transfer resistance of steel, and Q_{dl} is the double layer capacitance at the steel-solution interface. R_f and Q_f are the resistance and capacitance of the passive film, respectively. The constant phase element (CPE, expressed as Q) was used as an alternative to the pure capacitor to represent the non-homogeneity of steel surface. The low-frequency time constant ($R_{ct}Q_{dl}$) reflects the charge transfer process of steel electrode, and the high-frequency time constant (R_fQ_f) is associated with the redox reactions (Fe^{2+}/Fe^{3+}) of the passive film [31,34]. The impedance (Z_{CPE}) of Q_f and Q_{dl} can be expressed by Eq. (1).

$$Z_{CPE} = \frac{1}{Y_0}(j\omega)^{-n} \quad (1)$$

where admittance Y_0 and dispersion coefficient n are two CPE elements, and ω is the angular frequency. The apparent capacitance of Q_f and Q_{dl} is defined as follows [36,37]:

$$C_f = \frac{(Y_0(Q_f)\cdot R_f)^{1/n}}{R_f} \quad (2)$$

Table 2
Best fitting parameters of the impedance spectra.

Steel type	Passivation time	R_s (Ω cm^2)	High-frequency time constant			Low-frequency time constant		
			R_f (kΩ cm^2)	Y_0 (Q_f) (10^{-5} Ω^{-1} cm^{-2} s^n)	Q_f, n	R_{ct} (kΩ cm^2)	Y_0 (Q_{dl}) (10^{-5} Ω^{-1} cm^{-2} s^n)	Q_{dl}, n
LC	1 h	34.5	23.3	3.53	0.925	67.1	2.33	0.570
	10 d	32.1	82.7	2.79	0.935	348.1	2.00	0.926
LA	1 h	34.4	61.2	2.91	0.947	134.9	0.79	0.452
	10 d	34.3	342.6	2.59	0.966	436.5	0.78	0.817

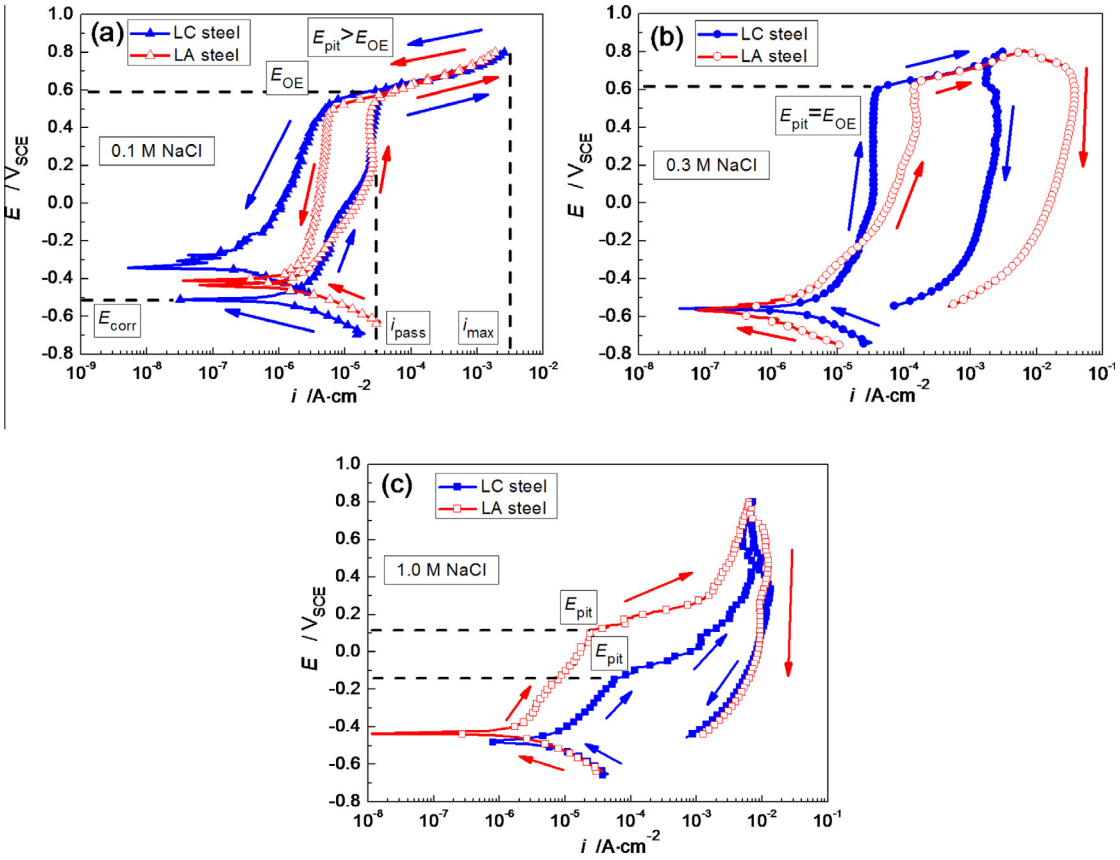

Fig. 4. CPP curves for LC and LA steels without passivation in SCPS with various chloride concentrations.

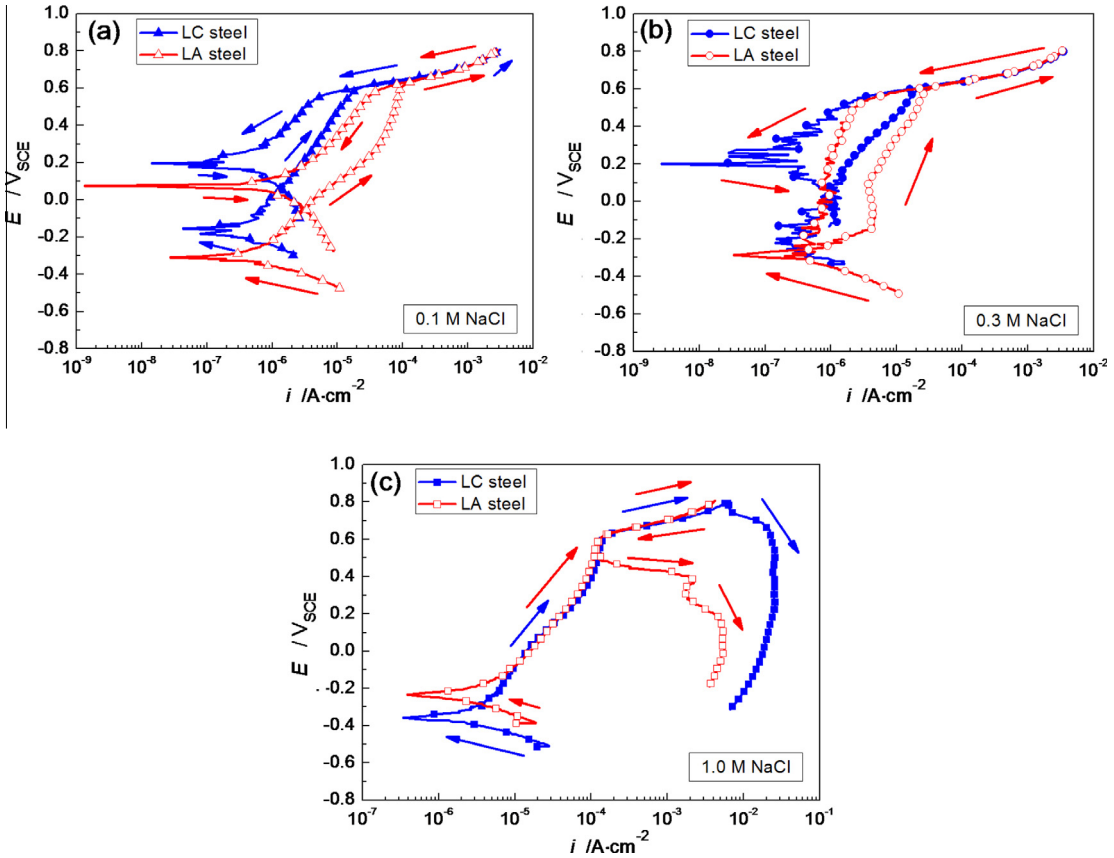

Fig. 5. CPP curves for LC and LA steels after 10 days of passivation in SCPS with various chloride concentrations.

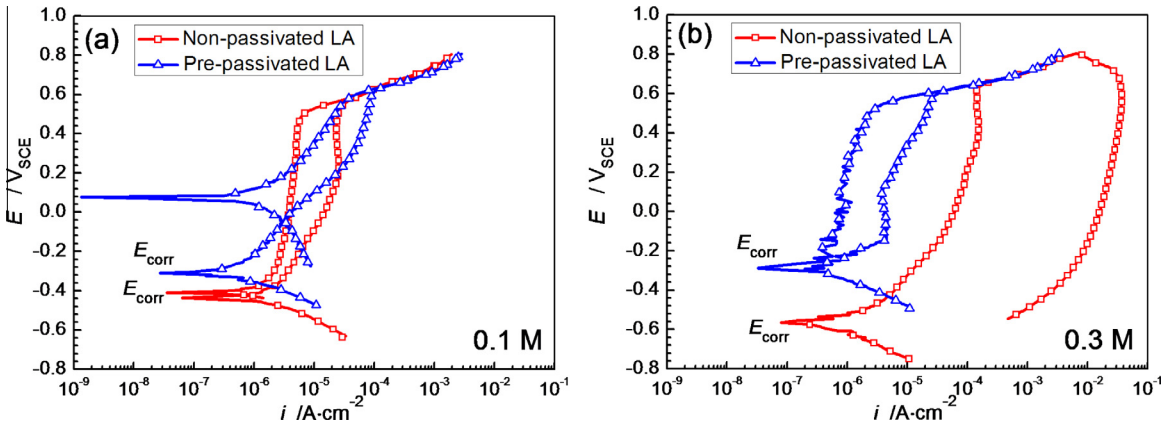

Fig. 6. The effect of passivation on the pitting corrosion behavior of LA steel in SCPS with 0.1 M and 0.3 M NaCl.

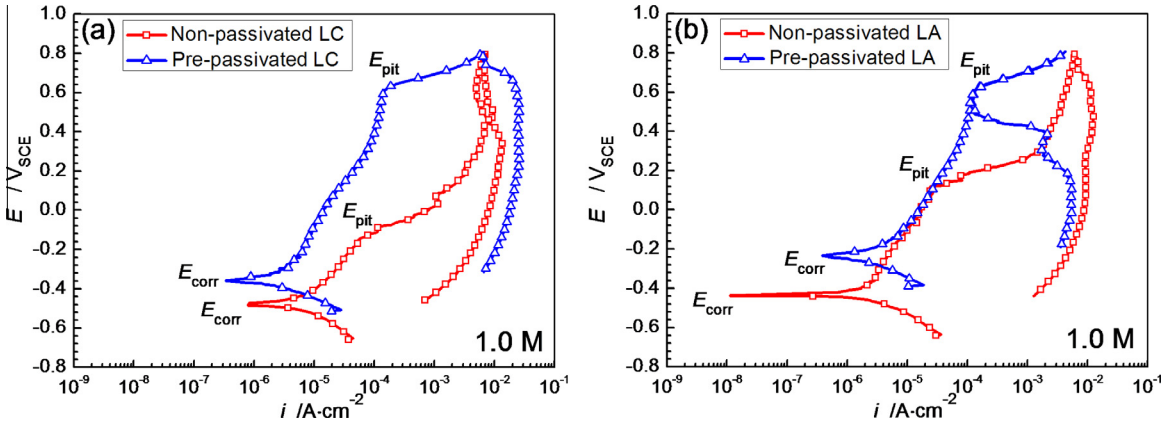

Fig. 7. The effect of passivation on the pitting corrosion behavior of LC and LA steels in SCPS with 1.0 M NaCl.

$$C_{dl} = \frac{(Y_0(Q_{dl}) \cdot R_{ct})^{1/n}}{R_{ct}} \quad (3)$$

The EIS parameters, fitted by software ZSimpWin, are presented in Table 2. The chi-square (χ^2) values are of the order of 10^{-4}–10^{-3} for all cases, indicating a good fit with this equivalent circuit, as shown in Fig. 2. It is worth noting from Table 2 that, the high-frequency time constant of passive film was similar to the low-frequency time constant of the charge transfer reaction. In general, the number of phase angle peaks is an indication of the number of time constants. However, in some cases the time constants may overlap each other [31]. Therefore, it is very difficult to separate them from the broad phase angle peak presented in Fig. 2c. It can be seen in Table 2 that, after 10 days of passivation, R_s is almost unchanged for both cases. R_f and R_{ct} are significantly increased for both LC and LA steels after 10 days of passivation. Meanwhile, $Y_0(Q_f)$ and $Y_0(Q_{dl})$ are slightly decreased. It indicates that passive film has been formed and the corrosion resistance of both steels is largely improved. In addition, it is evident that the corrosion resistance of the passive film for LA steel is slightly higher than LC steel, on the basis of the higher R_f and R_{ct} after 10 days of passivation in SCPS.

3.2. The effect of chloride concentration on pitting corrosion

3.2.1. Non-passivated steel

Fig. 4 presents the CPP curves of non-passivated steels exposed to SCPS with 0.1 M, 0.3 M and 1.0 M NaCl, respectively. At NaCl concentration of 0.1 M (Fig. 4a), the corrosion potential (E_{corr}) of LA steel is slightly higher than LC steel. However, upon further anodic polarization both steels show almost the same CPP curve. When the anodic polarization potential is above 0.1 V_{SCE}, the current density keeps constant, indicating the occurrence of passive region for both steels. It can be seen that the passive current density (i_{pass}) for both steels are ~3×10^{-5} A cm^{-2}. At the polarization potential of about 0.6 V_{SCE}, the sudden increase of current density for both steels can be observed. It is worth noting that 0.6 V_{SCE}, rather than the pitting potential (E_{pit}), should be the potential for oxygen evolution reaction (E_{OE}) in SCPS. This result is in good agreement with the previous investigations [21,24]. In this case, the true E_{pit} values for LC and LA steels are higher than E_{OE}. It was confirmed by Hurley and Scully [10] that for stainless steel, CPP measurement was ineffective for determining the chloride-induced pitting corrosion potential. The reason is that oxygen evolution occurred prior to the breakdown of passive film. When the potential reverses to the cathodic direction as shown in Fig. 4a, the corresponding current density of backward potential scan is lower than the forward scan. Therefore, it demonstrates that no pitting corrosion occurred for LC and LA steels when exposed to SCPS with 0.1 M NaCl, even if no passive film was formed in advance.

In SCPS with 0.3 M NaCl (Fig. 4b), both steels exhibit evident pitting corrosion behavior. It is clear that the i_{pass} value of LA steel is higher than that of LC steel. Moreover, the potential range of passivation for LA steel is much smaller compared with LC steel. After the passive region, sudden increase of current density for both steels can be observed. However, unlike the case of 0.1 M NaCl, the corresponding current density of backward potential scan of both steels is higher than the forward scan. Therefore, a positive hysteresis loop is formed, indicating the development of corrosion

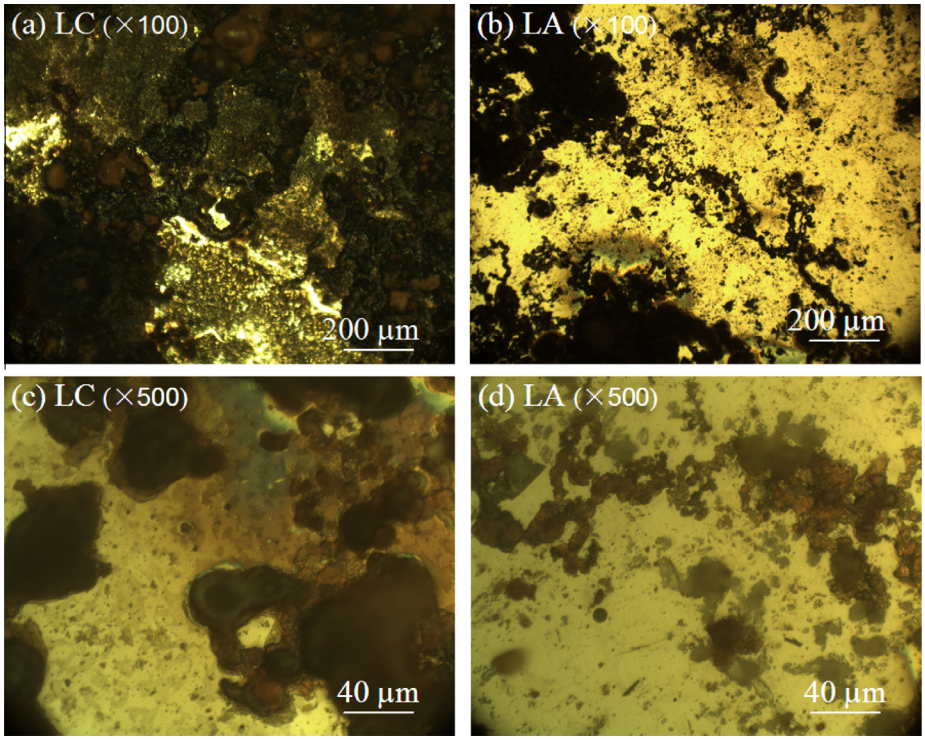

Fig. 8. Optical micrographs of pre-passivated steels after CPP measurements in SCPS with 1.0 M NaCl.

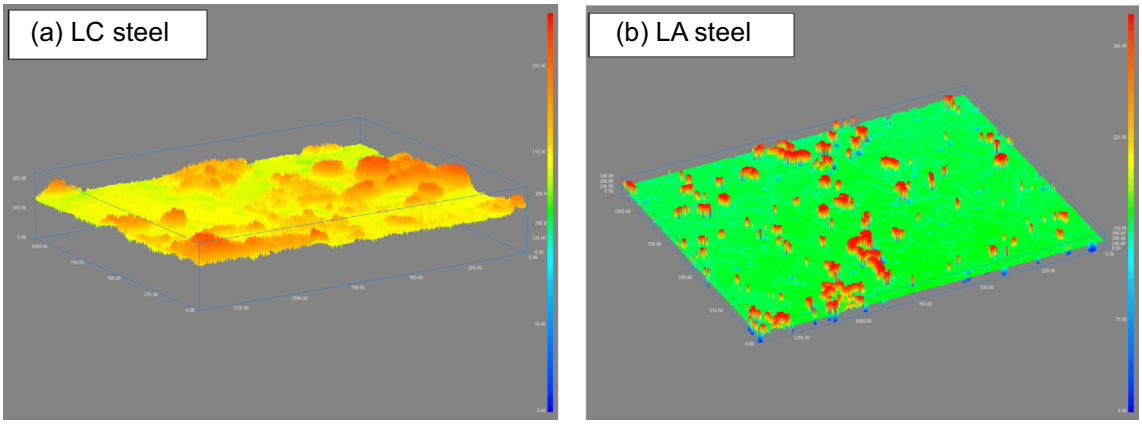

Fig. 9. CLSM images (1125 μm × 1375 μm) of pre-passivated steels after CPP measurements in SCPS with 1.0 M NaCl.

pits on steel surface [21,22]. It can be seen that the area of hysteresis loop for LA steel is somewhat larger than that of LC steel. If steels exhibit similar E_{pit} values, the area of the positive hysteresis loop can be used to quantify the pitting corrosion resistance [21]. On the basis of the CPP curves presented in Fig. 4b, it appears that the pitting corrosion resistance of LA steel is slightly lower than LC steel when exposed to 0.3 M NaCl.

It is can be seen from Fig. 4c that no clear passive region can be observed for both steels in SCPS with 1.0 M NaCl, suggesting the occurrence of severe pitting corrosion on steel surface. In addition, hysteresis loops occur for both steels. E_{corr} value of LA steel is more positive than that of LC steel, and the current density of the anodic polarization for LA steel is lower compared with LC steel. Furthermore, E_{pit} value of LA steel is approximately 0.1 V_{SCE}, whereas E_{pit} value of LC steel is lower than −0.1 V_{SCE}. In consequence, in SCPS with 1.0 M NaCl the pitting corrosion resistance of LA steel is superior to LC steel.

3.2.2. Pre-passivated steel

The pitting corrosion behaviors of naturally passivated steels in SCPS with various chloride concentrations are depicted in Fig. 5. When tested in SCPS with 0.1 M and 0.3 M NaCl, no pitting corrosion can be observed for LC and LA steels (Fig. 5a, b). It should be noted that the i_{pass} value of pre-passivated LA steel is higher than pre-passivated LC steel. Moreover, the E_{corr} value of LA steel is more negative than LC steel. This result is in accordance with the non-passivated case. In SCPS with 1.0 M NaCl (Fig. 5c), higher pitting corrosion resistance for LA steel is identified, since the area of the hysteresis loop of LA steel is much smaller than that of LC steel.

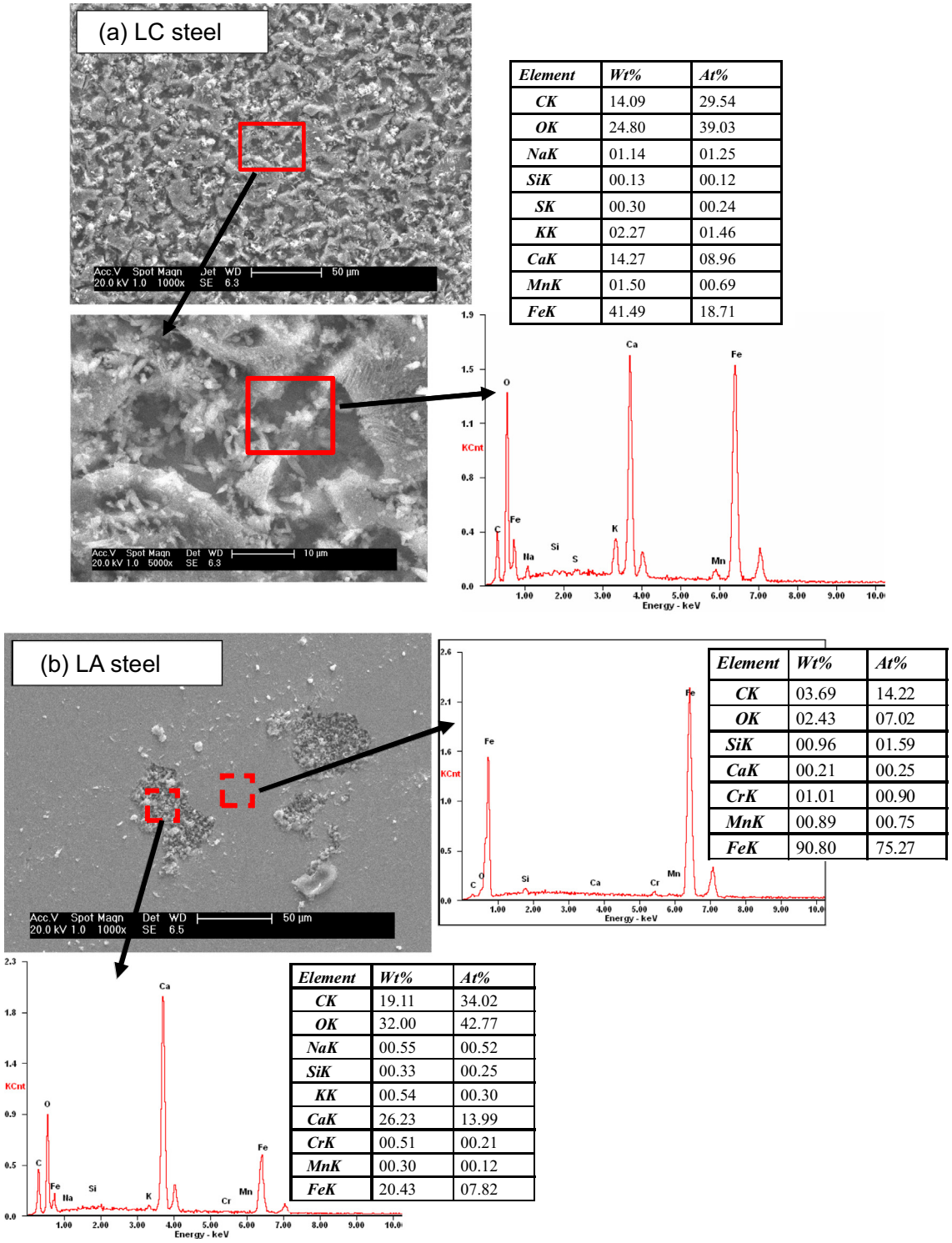

Element	Wt%	At%
CK	14.09	29.54
OK	24.80	39.03
NaK	01.14	01.25
SiK	00.13	00.12
SK	00.30	00.24
KK	02.27	01.46
CaK	14.27	08.96
MnK	01.50	00.69
FeK	41.49	18.71

Element	Wt%	At%
CK	03.69	14.22
OK	02.43	07.02
SiK	00.96	01.59
CaK	00.21	00.25
CrK	01.01	00.90
MnK	00.89	00.75
FeK	90.80	75.27

Element	Wt%	At%
CK	19.11	34.02
OK	32.00	42.77
NaK	00.55	00.52
SiK	00.33	00.25
KK	00.54	00.30
CaK	26.23	13.99
CrK	00.51	00.21
MnK	00.30	00.12
FeK	20.43	07.82

Fig. 10. SEM images and EDS of pre-passivated steels after CPP measurements in SCPS with 1.0 M NaCl.

According to the results of both non-passivated and pre-passivated cases, it is confirmed that LA steel exhibits even lower pitting corrosion resistance in SCPS with 0.1 M and 0.3 M NaCl, compared to LC steel. Two reasons are considered to be responsible for this difference. On the one hand, with the increase in ferrite phase in LA steel caused by the special heat treatment process, the potential difference between the ferrite phase and the pearlite phase is larger than that in LC steel. Therefore, it is easier for low-alloy steel to form microcells in chloride solutions, resulting in the lower initial corrosion resistance [16]. On the other hand, the lower pitting corrosion resistance of LA steel may also result from the large grain size. It was claimed that, with the increase of grain size the local corrosion near the grain boundary was increased due to the increase of local corrosion current density [9,38]. However, at high NaCl concentration of 1.0 M, higher pitting corrosion resistance has been recorded for LA steel. This result is in good agreement with that of Singh and Singh [7] and Hussain et al. [8]. They found that low-alloy steel had lower initial corrosion

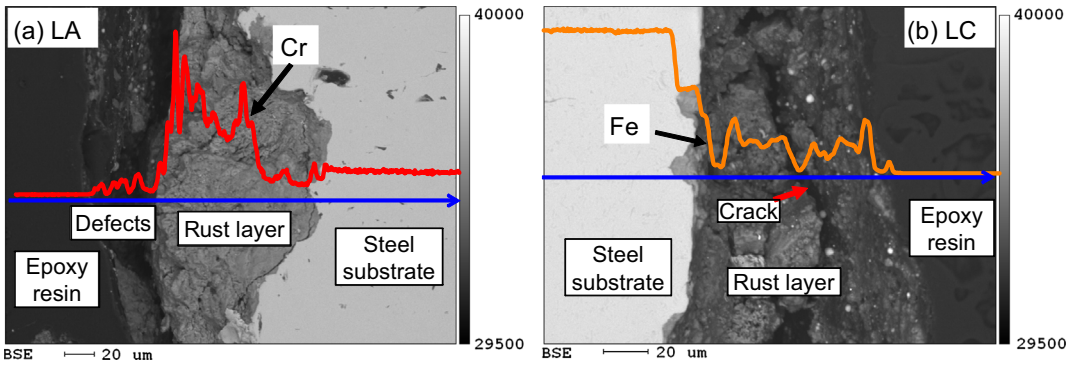

Fig. 11. EPMA images for the distribution of characteristic elements in the substrate and rust layer of steels.

resistance in comparison to low-carbon steel or TMT steel. However, with the exposure time low-alloy steel dominated over the other two steels, probably owing to the gradual formation of dense Cr-bearing rust layer inside corrosion pits or on steel surface.

3.3. The effect of pre-passivation on pitting corrosion

Fig. 6 shows the comparison of the pitting corrosion resistance of non-passivated and pre-passivated LA steel in SCPS with 0.1 M and 0.3 M NaCl. It can be seen in Fig. 6a that there is no trace of pitting corrosion with 0.1 M NaCl for both cases. However, E_{corr} value for LA steel is significantly increased after the formation of passive film. For the case of 0.3 M NaCl (Fig. 6b), the improved pitting corrosion resistance for pre-passivated LA steel is more pronounced. Compared with non-passivated LA steel, much more positive E_{corr} value and lower passive current density can be observed for pre-passivated LA steel. In addition, a large positive hysteresis loop is formed for non-passivated steel, whereas there is no indication of pitting corrosion for pre-passivated steel. The similar trend was observed for LC steel in SCPS with 0.1 M and 0.3 M NaCl. It is evident from Fig. 7 that more positive E_{corr} and E_{pit} values can be identified for pre-passivated steels than non-passivated cases in SCPS with 1.0 M NaCl. Moreover, pre-passivated steels also exhibit smaller positive hysteresis loops.

According to the CPP curves in Figs. 6 and 7, it is evident that pre-passivation in chloride-free SCPS can improve the pitting corrosion resistance significantly for LC and LA steels at all chloride concentrations. Li and Sagüés [18] found that the passive film formed on low-carbon steel by pre-passivation could increase E_{pit} values significantly. However, it did not significantly change the spread of the pitting probability distribution. Enrico et al. [19] also identified that, naturally grown oxide layer significantly affected the electrochemical response of the steel surface by hindering the charge transfer mechanism.

3.4. Surface morphology of corrosion products and corrosion pits

The optical micrographs of pre-passivated LC and LA steels after CPP measurements with 1.0 M NaCl can be seen in Fig. 8. The surface of LC steel is covered with widespread and overlapped corrosion products (Fig. 8a, c), indicating severe pitting corrosion induced by chlorides. However, only sparse pitting can be observed for LA steel (Fig. 8b, d). Fig. 9 exhibits 3D images of the surface morphology of steels after CPP measurements in SCPS with 1.0 M NaCl. For LC steel (Fig. 9a), there is a large amount of corrosion products on steel surface. Most of the corrosion pits are filled or covered with corrosion products. Compared with LC steel, few corrosion products can be observed on the surface of LA steel (Fig. 9b), and most of the corrosion pits are partially filled with corrosion products.

Fig. 10 shows SEM images of pre-passivated steels after CPP measurements in SCPS with 1.0 M NaCl. It can be seen in Fig. 10a that the substrate of LC steel is covered with widespread porous corrosion products. The result of EDS indicates that the content of element O is higher and element Fe is relatively lower in comparison to the chemical composition of LC steel substrate. It is clear from Fig. 10a that the content of element Ca is very high. On the one hand, excessive $Ca(OH)_2$ may deposit on the surface of the corrosion products as well as inside the pores and microcracks of corrosion products. On the other hand, Ca may participate in the formation of corrosion products, probably $CaFe_2O_4$, which was proposed by Duffo et al. [39] and Koleva [40].

Unlike LC steel, only dispersive corrosion pits could be observed on the surface of LA steel (Fig. 10b). These corrosion pits are filled with corrosion products and white deposits. It can be seen from EDS results that, like the case of LC steel, the content of element Ca is high inside the pits of LA steel. Therefore, it suggests that the white deposits inside corrosion pits are Ca-containing substances, which may inhibit the propagation and the accumulation of corrosion products and further prevent the attack of chloride ions [40]. It should be noted that due to the formation of white deposits the content of Cr inside pits, as shown in Fig. 10b, is slightly lower than in steel substrate. Indeed, the corrosion products of LA steel are enriched with Cr, as shown in Fig. 11a. The peak of Cr was detected within the rust layer of LA steel, so that compact and dense rust layer, likely composed of α-$Fe_xCr_{1-x}OOH$, was formed inside corrosion pits [41]. On the contrary, relatively loose rust layer with cracks was observed for LC steel, as shown in Fig. 11b. Thus, the formation of Cr-enriched rust layer at high NaCl concentration contributes to the high pitting corrosion resistance of LA steel.

4. Conclusions

From the results of above investigations, the following conclusions can be drawn:

1. Passive film formed on steel surface could improve the chloride-induced pitting corrosion resistance of both LA and LC steels in simulated concrete pore solution with various chloride concentrations.
2. The inferior pitting corrosion resistance of LA steel exposed to simulated concrete pore solution with 0.1 M and 0.3 M NaCl may be accounted for from its microstructure. The large ferrite phase in LA steel leads to the easier formation of microcells and higher local corrosion current density near the grain boundary than that in LC steel.

3. When NaCl concentration was increased to 1.0 M in simulated concrete pore solution, LA steel exhibited superior pitting corrosion resistance than LC steel. The main reason is that the gradually formed compact Cr-enriched rust layer in LA steel can effectively suppress the propagation of corrosion pits.

Acknowledgments

The authors greatly acknowledge support provided by the National Natural Science Foundation of China (No. 51208098), the 973 Project (No. 2015CB655100) and the Industry-University Research Cooperative Innovation Fund of Jiangsu Province (No. BY2013091).

References

[1] G.S. Duffó, M. Reinoso, C.P. Ramos, S.B. Farina, Characterization of steel rebars embedded in a 70-year old concrete structure, Cem. Concr. Res. 42 (1) (2012) 111–117.
[2] I. Khan, R. François, A. Castel, Prediction of reinforcement corrosion using corrosion induced cracks width in corroded reinforced concrete beams, Cem. Concr. Res. 56 (2014) 84–96.
[3] M.C. García-Alonso, J.A. González, J. Miranda, M.L. Escudero, M.J. Correia, M. Salta, A. Bennani, Corrosion behaviour of innovative stainless steels in mortar, Cem. Concr. Res. 37 (11) (2007) 1562–1569.
[4] C.M. Abreu, M.J. Cristóbal, M.F. Montemor, X.R. Nóvoa, G. Pena, M.C. Pérez, Galvanic coupling between carbon steel and austenitic stainless steel in alkaline media, Electrochim. Acta 47 (13) (2002) 2271–2279.
[5] D.D.N. Singh, R. Ghosh, Unexpected deterioration of fusion-bonded epoxy-coated rebars embedded in chloride-contaminated concrete environments, Corrosion 61 (8) (2005) 815–829.
[6] F. Presuel-Moreno, J.R. Scully, S.R. Sharp, Literature review of commercially available alloys that have potential as low-cost, corrosion-resistant concrete reinforcement, Corrosion 66 (8) (2010) 0860011–08600113.
[7] J.K. Singh, D.D.N. Singh, The nature of rusts and corrosion characteristics of low alloy and plain carbon steels in three kinds of concrete pore solution with salinity and different pH, Corros. Sci. 56 (2012) 129–142.
[8] R.R. Hussain, A. Alhozaimy, A. Al-Negheimish, D. Singh, Time-dependent variation of the electrochemical impedance for thermo-mechanically treated versus plain low alloy steel rebars in contact with simulated concrete pore solution, Constr. Build. Mater. 73 (2014) 283–288.
[9] M. Hegazy, M. Eissa, Influence of microalloying on the corrosion resistance of steel in saturated calcium hydroxide, Metall. Mater. Trans. A 27 (6) (1996) 1701–1707.
[10] M.F. Hurley, J.R. Scully, Threshold chloride concentrations of selected corrosion-resistant rebar materials compared to carbon steel, Corrosion 62 (10) (2006) 892–904.
[11] A. Ray, D. Mukerjee, S. Sen, A. Bhattacharya, S. Dhua, M. Prasad, N. Banerjee, A. Popli, A. Sahu, Microstructure and properties of thermomechanically strengthened reinforcement bars: a comparative assessment of plain-carbon and low-alloy steel grades, J. Mater. Eng. Perform. 6 (3) (1997) 335–343.
[12] B. Panigrahi, S. Srikanth, G. Sahoo, Effect of alloying elements on tensile properties, microstructure, and corrosion resistance of reinforcing bar steel, J. Mater. Eng. Perform. 18 (8) (2009) 1102–1108.
[13] G. Sahoo, R. Balasubramaniam, On the corrosion behaviour of phosphoric irons in simulated concrete pore solution, Corros. Sci. 50 (1) (2008) 131–143.
[14] G. Sahoo, R. Balasubramaniam, S. Misra, Corrosion of phosphoric irons in cement grout, Corrosion 63 (10) (2007) 975–982.
[15] M. Liu, X. Cheng, X. Li, Z. Jin, H. Liu, Corrosion behavior of Cr modified HRB400 steel rebar in simulated concrete pore solution, Constr. Build. Mater. 93 (2015) 884–890.
[16] D. Trejo, P.J. Monteiro, Corrosion performance of conventional (ASTM A615) and low-alloy (ASTM A706) reinforcing bars embedded in concrete and exposed to chloride environments, Cem. Concr. Res. 35 (3) (2005) 562–571.
[17] D.D.N. Singh, T. Venugopalan, Understanding the corrosion and remedial measures to control the deterioration of reinforcement steel bars by modification in their chemistry and application of surface coatings, Trans. Indian Inst. Met. 66 (5–6) (2013) 677–687.
[18] L. Li, A. Sagues, Chloride corrosion threshold of reinforcing steel in alkaline solutions-cyclic polarization behavior, Corrosion 58 (4) (2002) 305–316.
[19] E. Volpi, A. Olietti, M. Stefanoni, S.P. Trasatti, Electrochemical characterization of mild steel in alkaline solutions simulating concrete environment, J. Electroanal. Chem. 736 (2015) 38–46.
[20] M. Ormellese, L. Lazzari, S. Goidanich, G. Fumagalli, A. Brenna, A study of organic substances as inhibitors for chloride-induced corrosion in concrete, Corros. Sci. 51 (12) (2009) 2959–2968.
[21] R.D. Moser, P.M. Singh, L.F. Kahn, K.E. Kurtis, Chloride-induced corrosion resistance of high-strength stainless steels in simulated alkaline and carbonated concrete pore solutions, Corros. Sci. 57 (2012) 241–253.
[22] M. Saremi, E. Mahallati, A study on chloride-induced depassivation of mild steel in simulated concrete pore solution, Cem. Concr. Res. 32 (12) (2002) 1915–1921.
[23] O. Rosas, E. Maya-Visuet, H. Castaneda, Effect of chloride ions on the electrochemical performance of LDX 2003 alloy in concrete and simulated concrete-pore solutions, J. Appl. Electrochem. 44 (5) (2014) 631–646.
[24] S. Alvarez, A. Bautista, F. Velasco, Corrosion behaviour of corrugated lean duplex stainless steels in simulated concrete pore solutions, Corros. Sci. 53 (5) (2011) 1748–1755.
[25] S. Fajardo, D.M. Bastidas, M. Criado, M. Romero, J. Bastidas, Corrosion behaviour of a new low-nickel stainless steel in saturated calcium hydroxide solution, Constr. Build. Mater. 25 (11) (2011) 4190–4196.
[26] A. Poursaee, Corrosion of steel bars in saturated $Ca(OH)_2$ and concrete pore solution, Cem. Concr. Lett. 1 (3) (2010) 90–97.
[27] A. Poursaee, C. Hansson, Reinforcing steel passivation in mortar and pore solution, Cem. Concr. Res. 37 (7) (2007) 1127–1133.
[28] P. Ghods, O. Isgor, G. McRae, G. Gu, Electrochemical investigation of chloride-induced depassivation of black steel rebar under simulated service conditions, Corros. Sci. 52 (5) (2010) 1649–1659.
[29] A. Al-Negheimish, A. Alhozaimy, R.R. Hussain, R. Al-Zaid, J. Singh, D. Singh, Role of manganese sulfide inclusions in steel rebar in the formation and breakdown of passive films in concrete pore solutions, Corrosion 70 (1) (2013) 74–86.
[30] L. Freire, M. Carmezim, M. Carmezim, Ma Ferreira, M. Montemor, The passive behaviour of AISI 316 in alkaline media and the effect of pH: a combined electrochemical and analytical study, Electrochim. Acta 55 (21) (2010) 6174–6181.
[31] C.Q. Ye, R.G. Hu, S.G. Dong, X.J. Zhang, R.Q. Hou, R.G. Du, C.J. Lin, J.S. Pan, EIS analysis on chloride-induced corrosion behavior of reinforcement steel in simulated carbonated concrete pore solutions, J. Electroanal. Chem. 688 (2013) 275–281.
[32] F. Zhang, J.S. Pan, C.J. Lin, Localized corrosion behaviour of reinforcement steel in simulated concrete pore solution, Corros. Sci. 51 (9) (2009) 2130–2138.
[33] J.C. Zhang, W.K. Huang, H. Ma, Microstructure and properties of 20MnSiCrV corrosion resistant rebar in continuous cooling transformation, Hot Work Technol. 43 (6) (2014) 91–95.
[34] Y. Morozov, A. Castela, A. Dias, M. Montemor, Chloride-induced corrosion behavior of reinforcing steel in spent fluid cracking catalyst modified mortars, Cem. Concr. Res. 47 (2013) 1–7.
[35] J. Hu, D. Koleva, J. De Wit, H. Kolev, K. Van Breugel, Corrosion performance of carbon steel in simulated pore solution in the presence of micelles, J. Electrochem. Soc. 158 (3) (2011) C76–C87.
[36] F. Tang, X. Cheng, G. Chen, R.K. Brow, J.S. Volz, M.L. Koenigstein, Electrochemical behavior of enamel-coated carbon steel in simulated concrete pore water solution with various chloride concentrations, Electrochim. Acta 92 (2013) 36–46.
[37] M. Pech-Canul, P. Castro, Corrosion measurements of steel reinforcement in concrete exposed to a tropical marine atmosphere, Cem. Concr. Res. 32 (3) (2002) 491–498.
[38] B. Wang, Q.Y. Liu, X.D. Wang, Effect of grain size on atmospheric corrosion resistance of ultra-low carbon IF steel, Acta Metall. Sin. 48 (5) (2012) 601–606.
[39] G. Duffo, W. Morris, I. Raspini, C. Saragovi, A study of steel rebars embedded in concrete during 65 years, Corros. Sci. 46 (9) (2004) 2143–2157.
[40] D.A. Koleva, Electrochemical behavior of corroded and protected construction steel in cement extract, Mater. Corros. 62 (3) (2011) 240–251.
[41] Q.C. Zhang, J.S. Wu, J.J. Wang, W.L. Zheng, J.G. Chen, A.B. Li, Corrosion behavior of weathering steel in marine atmosphere, Mater. Chem. Phys. 77 (2) (2003) 603–608.